# Scattering control based on geometric phase reflection-type coded metasurface

BIN LOU[1], JIANFENG XU[2], FUHAI LIU[2], LIZHEN XU[3], BO FANG[4,*]
[1]*Jiaxing Nanyang Polytechnic Institute, Jiaxing, China*
[2]*Special Equipment College, Hangzhou Vocational & Technical College, Hangzhou 310018, China*
[3]*College of Information Engineering, Hangzhou Vocational & Technical College, Hangzhou 310018, China*
[4]*College of Metrology & Measurement Engineering, China Jiliang University, Hangzhou 310018, China*

We propose a metal-media-metal reflective cell structure to construct a coded metasurface. The metal material is gold, the medium material is polyimide, and the frequency range of operation is 0.2 THz-0.8 THz. Using the Pancharatnam-Berry phase principle, the continuous change of reflection phase is realized by rotating the anisotropic strip structure. We designed 4 unit structures with phase intervals of 90°. They are arranged in a certain sequence into a phase-gradient array to construct a coded metasurface reflection structure. Through different coding sequences, different abnormal reflection angles can be realized. By using the full wave simulation method, we calculated the scattering angles and scattering efficiency of different sequences. In order to realize the continuous control of the angle of reflection and scattering, we introduce the Fourier code addition principle in digital signal processing. By adding different sequences of encoded particles, a new encoding sequence can be obtained, and the scattering angle can be controlled freely.

(Received October 18, 2023; accepted April 8, 2024)

*Keywords:* Metasurface, Metamaterials, Optics devices

## 1. Introduction

Metamaterials are a new kind of man-made materials. Unlike traditional materials, metamaterials have many advantages in electromagnetic properties. This kind of material can adjust the amplitude, polarization and phase of electromagnetic wave and other related parameters in a more comprehensive way, and can realize the functions that are difficult to achieve in some aspects of traditional materials [1-10]. Metamaterials is a burgeoning discipline and a novel interdisciplinary field. There is a lot of research going on around metamaterials, such as "invisibility cloaks" at different wavelengths, electromagnetic black holes, terahertz imaging and detection techniques, real-time information processing systems, and more [11-20].

Metasurface can be seen as the two-dimensional counterpart of metamaterials, not really two-dimensional structure, but refers to its thickness is generally very thin [21]. A series of subwavelength unit structures are arranged on the plane according to a certain periodic law, or aperiodic arrangement, and the planar structure is formed when the thickness is less than the working wavelength. When the length, width and height of the basic unit of the metasurface are changed, various physical and electromagnetic properties of the metasurface will be changed accordingly, and flexible control can be achieved in this way. It can be said that the study of metasurface opens up a new way in the study of electromagnetic wave regulation.

In 2014, Professor Cui Tiejun proposed the concept of coded metasurface, which is essentially the use of digital states to characterize electromagnetic information [22], combining digital technology at the information level with metamaterial technology at the physical level, so that electromagnetic parameters can be more easily regulated and the research of metasurface can be more convenient to operate [23-30]. The advantage of coded metasurfaces stems from the ease of incorporating digital technology. The unit structure of the coded metasurface comes from the all-phase bisection, so if the bisection angle is too small, it will lead to too much unit structure, which increases the computational difficulty of the research [31-44]. On the other hand, it can be seen that the phase control of the unit structure obtained in this way is discrete, and the study of continuous phase control cannot be realized.

Here, a metal-media-metal reflecting element structure is proposed to construct a coded metasurface. The metal material is gold, the medium material is polyimide, and the frequency range of operation is 0.2 THz-0.8 THz. Using the Pancharatnam-Berry phase principle, the continuous change of reflection phase is

realized by rotating the anisotropic strip structure.

## 2. Theoretical analysis

The geometric phase principle can also be called the Pancharatnam−Berry (PB) phase principle, which is in honor of the British scientist Berry and Indian scientist Pancharatnam who discovered this principle. When a beam of circularly polarized light is incident on the surface, the reflected light or transmitted light will appear cross-polarized components. The corresponding cross-polarized components will be accompanied by phase delay phenomenon. It is found that if the rotation angle of the structure is $\theta$, the phase changes is $2\theta$ or $-2\theta$. That is, the value of the phase change is always twice the value of the structure rotation angle.

Coded metasurface elements can be constructed using geometric phases. The coded metasurface can have 1-bit, 2-bit, 3-bit, 4-bit.... Taking 2-bit coded metasurface as an example, 0° phase can be represented by the number "0", then the 90° phase is represented by the number "1", the 180° phase is represented by the number "2", and the 270° phase is represented by the number "3". The phase difference between the two units is 90°.

In the case of a 3-bit coded metasurface, there are a total of eight different phase cell structures, respectively, as 0°, 45°, 90°, 135°, 180°, 225°, 270° and 315°, which are numerically represented as "0", "1", "2", "3", "4", "5", "6" and "7". Obviously, with different bits, the number of unit structures on the metasurface is different, so the encoded metasurface with different bits can be flexibly selected according to the research needs, so as to achieve more accurate regulation of various electromagnetic waves.

The expression of the grating equation is [22]

$$\sin\theta_n - \sin\theta_i = n\frac{\lambda}{\tau} \tag{1}$$

where, $\theta_n$represents the diffraction angle of the $n$ order diffracted light, $\theta_i$represents the incident angle of the incident light, $n$ is the diffraction order, $\lambda$ is the wavelength of the incident light, and $\tau$ is the period of grating. When the incident angle of the incident light is 0°, obviously the diffraction angle of the first order diffracted light can be expressed as

$$\sin\theta = \frac{\lambda}{\tau} \tag{2}$$

The superelements are formed by geometric phase optimization and combination arrangement, whose diffraction characteristics are consistent with the grating equation. Suppose one have multiple superunits as K1, K2, K3... The period of each superunit is defined as $\tau 1, \tau 2, \tau 3$ …… The diffraction equation for each superelement can be expressed in eq. (2). Now by adding and subtracting the diffraction equations of different superelements, a new equation is obtained as

$$\sin\theta_m = \sin\theta_{K1} \pm \sin\theta_{K2} \pm \cdots \pm \sin\theta_{Kn} = \frac{\lambda}{\tau_1} \pm \frac{\lambda}{\tau_2} \pm \cdots \pm \frac{\lambda}{\tau_n} \tag{3}$$

Using the above formula, we can further obtain

$$\frac{1}{\tau_m} = \frac{1}{\tau_1} \pm \frac{1}{\tau_2} \pm \cdots \pm \frac{1}{\tau_n} \tag{4}$$

Now the grating composed of two super elements is added or subtracted, and the corresponding situation is shown in Fig. 1 [23-26]. It is not difficult to see from Fig. 1 that the addition principle can be performed according to the corresponding raster encoding, such as $0+0=0$, $0+1=1$, $0+2=2$, $1+1=2$, $1+2=0$. Based on the above principle, when any number of super elements with varying period lengths can be added or subtracted to obtain a new super element. If there is another super element with a period length that satisfies formula (4), the first order diffraction direction of the two super elements is the same. It is worth noting that the superunit constructed by this addition principle can realize the modulation of any angle, which overcomes the defect that only discrete angle regulation can be carried out when only geometric phase principle is used.

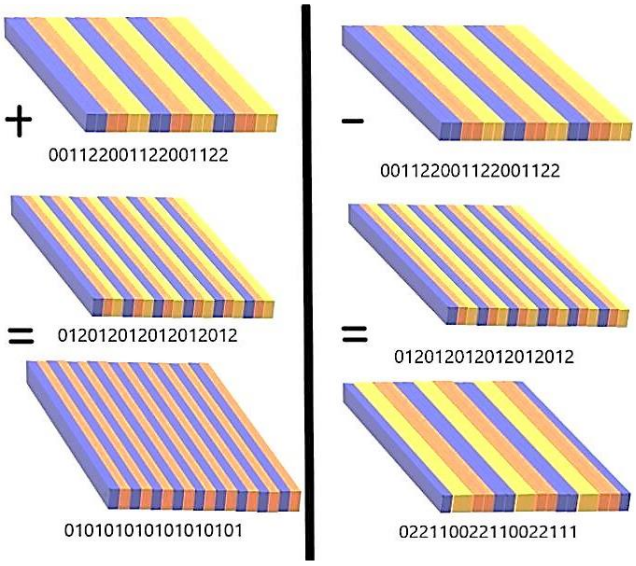


*Fig. 1. The grating is added or subtracted to create a new grating diagram (color online)*

## 3. Metasurface design

Fig. 2 shows the model of the unit structure, the yellow part is the metal material as gold, the blue part is the dielectric material Polyimide (dielectric constant: 3.5), the lower right part of the figure is the coding metasurface, and the upper left part is the structure diagram of a single coding particle in the metasurface. In the actual design, the

length and width of the underlying metal and the medium layer are the same, which is convenient to use the geometric phase principle to ensure that the phase change and the angle change are twice the relationship in value. The side length of the square unit structure is $L1 = 200\,\mu m$, the thickness of the bottom layer is $D3 = 0.2\,\mu m$, the thickness of the medium layer is $D2 = 50\,\mu m$, the length of the uppermost metal strip is $W = 110\,\mu m$, the width is $L = 20\,\mu m$, and the thickness is $D1 = 0.2\,\mu m$. In order to ensure the accuracy of geometric phase and design a unit structure with high reflection coefficient, it is necessary to pay attention to whether the phase difference of the reflected phase is 180° after the two linearly polarized light waves (X-axis polarization and Y-axis polarization) are incident on the vertical surface, and the reflected light in both polarization directions has a high reflection coefficient.

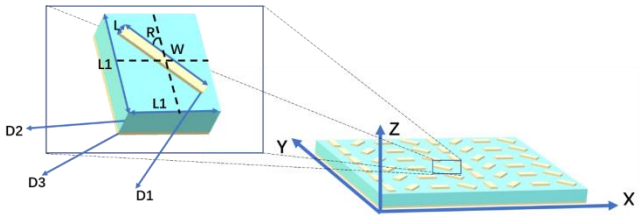


*Fig. 2. Metasurface and unit structure diagram (color online)*

In the design process, we used the full-wave simulation method to carry out parameter scanning to observe the change of S parameter. The S-parameter is the scattering parameter. It is an important parameter in microwave transmission. S12 is the reverse transmission coefficient, which is isolation. S21 is the forward transmission coefficient, that is, the gain. S11 is the input reflection coefficient, which is the input return loss, and S22 is the output reflection coefficient, which is the output return loss. Set the objective function to observe the reflected phase difference as close as possible to the 180° phase difference. Fig. 3 and Fig. 4 show the relationship between the phase difference after parameter scanning. In Fig. 3, different curves indicate different phase variations. Different numbers represent different units. In Fig. 4, different curves show the phase as a function of L. In the actual analysis, we optimize to obtain a purple line with a phase difference of -180° at a frequency of about 0.755THz. Fig. 5 reflects the reflection coefficient from the S-parameter. We used the finite integral method to numerically simulate the reflection coefficient and reflection phase of the element structure. It can be seen from Fig. 5 that the reflected light in both polarization directions has a high reflection coefficient in the frequency range of 0.2 THz-0.8 THz. After optimization, we can obtain the length of the uppermost metal strip is $W = 110\,\mu m$, and the width is $L = 20\,\mu m$.

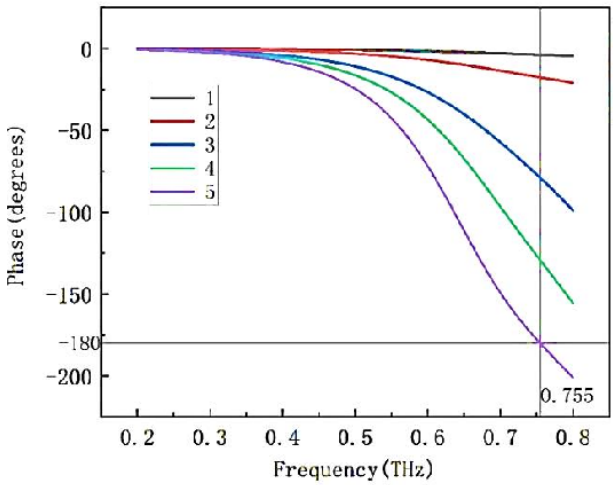


*Fig. 3. The variation of the reflection phase of the unit structure caused by different W values (color online)*

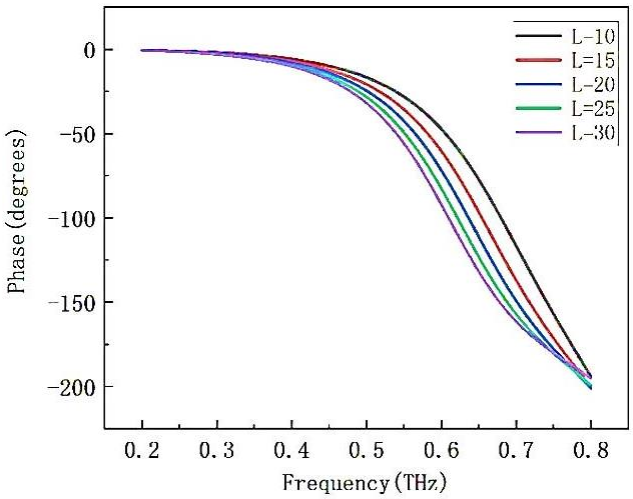


*Fig. 4. The variation of the reflection phase of the unit structure caused by different L values (color online)*

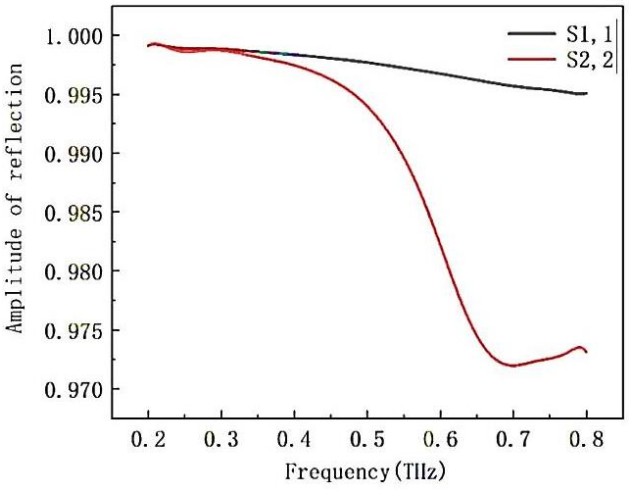


*Fig. 5. Reflection amplitudes of different incident polarizations (color online)*

Next, we change the incident polarized wave to a circularly polarized incident wave. We analyze the reflection phase and reflection amplitude of the periodic element structure. We define the rotation angle of the designed anisotropic element structure as R. By setting the rotation angle to a different angle, we can obtain the reflection amplitude and reverse phase of cross polarization at different angles, as shown in Fig. 6 and Fig. 7, respectively.

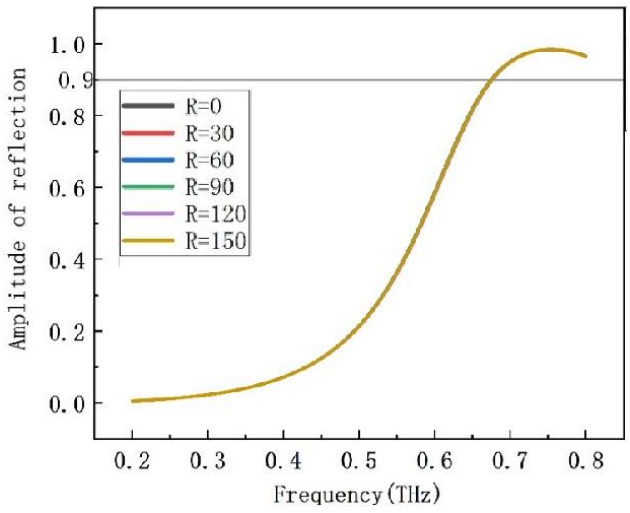


*Fig. 6. Effect of different rotation angles on reflection amplitude of cross circular polarization (color online)*

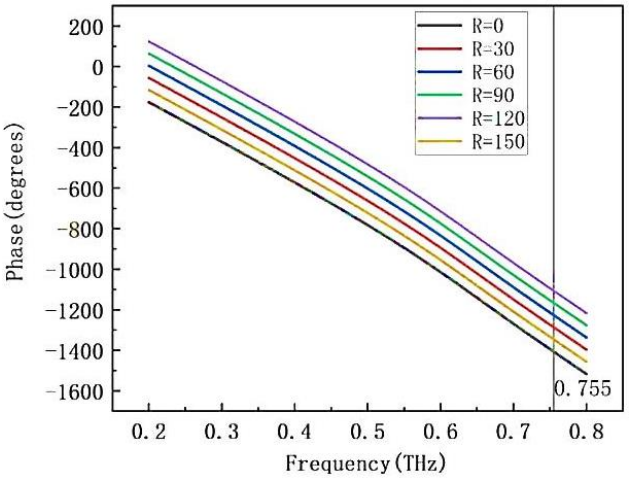


*Fig. 7. The influence of different rotation angles on the reflection phase of cross circular polarization (color online)*

We arrange these coding units into coding metasurfaces according to certain rules. Before using the addition principle, you first need to set up a basic coded metassurface. A phase gradient coded metasurface is designed as shown in Fig. 8(a) below, and its corresponding coding distribution is shown in Fig. 9(b). This is the full phase quartered, "0", "1", "2", "3" representing rotation angles of 0°, 45°, 90°, 135° , respectively. The sequence of the basic coded metasurface superunits is denoted as $S_0$, and the composed coded metasurface is composed of 50*10 unit structures. According to the generalized refraction and reflection law, the period of the grating is $\tau_1 = 6 \times 200\ \mu m = 1200\ \mu m$, the operating frequency is 0.755THz. According to $\theta = \sin^{-1}\frac{\lambda}{\tau}$, the reflected far-field scattering angle of the coded metasurface is $\theta \approx 19°$.

We need to ensure that the coded metasurface designed using the addition principle has the same diffraction angle as the basic coded metasurface, and that the metasurface contains exactly the same number of encoded particles. Two encoding metasurface supercells are constructed, which are $S_1 = 00112233\ldots\ldots$ and $S_2 = 000000111111222222333333\ldots\ldots$, respectively. Adding $S_1$ to $S_2$ yields the new superunit sequence $S_m = 001122\ldots\ldots$ as shown in Fig. 8(b). $S_0$ and $S_m$ have the same cycle length to ensure the same reflection angle at the same working frequency. Fig. 9 shows the arrangement of coding units and the corresponding far-field scattering characteristics of $S_0$ and $S_m$. $S_0$ is the basic coding sequence, and $S_m$ is the coding sequence constructed by addition principle. Their far-field scattering angles are basically the same, and the scattering efficiency of $S_m$ sequence is slightly higher than that of $S_0$ sequence. The metasurface constructed by addition principle achieves the expected goal of improving reflection efficiency.

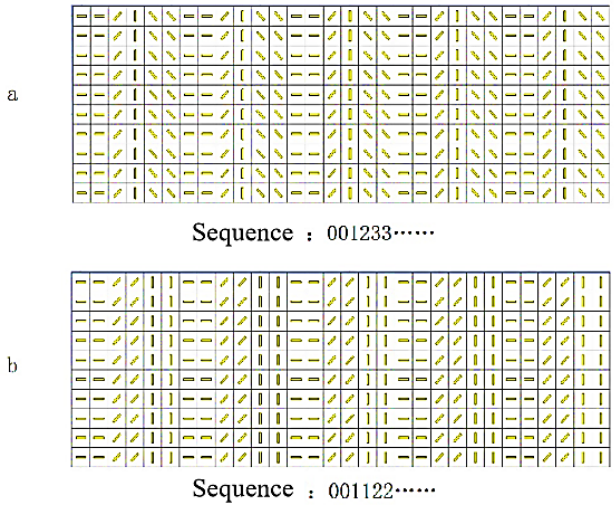


*Fig. 8. The basic sequence encoding metasurface $S_0$ and $S_m$*

To ensure the accuracy of the study, multiple sets of comparative simulations were conducted. In the second set of simulation, the period length of the basic grating is changed and the 360° phase is divided into six equal parts, that is, the coding numbers are changed into "0", "1",

"2", "3", "4" and "5". We further design two encoding metasurface as $S_0 = 000112345\ldots\ldots$ and $S_m = 001122445500223344\ldots\ldots$. $S_m$ can be realized by adding $S_1 = 001122334455\ldots\ldots$ and $S_2 = 000000111111222222333333444444555555\ \ldots\ldots$

According to encoding addition principle, the encoding sequence $S_m$ can be obtained. Although the encoding period for $S_0$ and $S_m$ is different, the diffraction angle is same according to the Generalized Snell's law. The calculated diffraction angle is 12.75°.

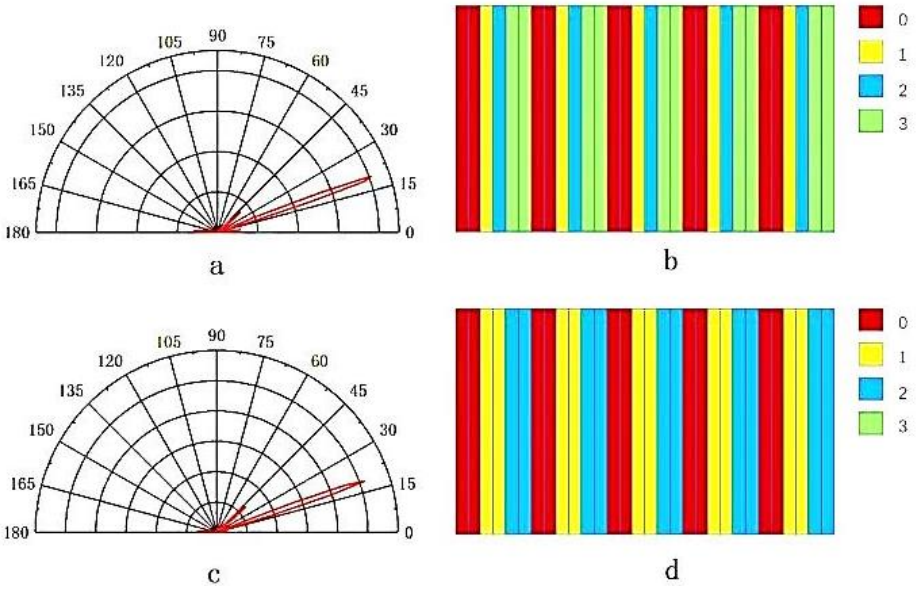


*Fig. 9. The basic sequence encodes the cell arrangement and the corresponding far-field scattering. (a) Far-field scattering of $S_0$, (b) Coding unit arrangement of $S_0$, (c) Far-field scattering of $S_m$, (d) Coding unit arrangement of $S_m$ (color online)*

Fig. 10 is a comparison of the second set of simulations. The upper part is the far-field scattering diagram a of the sequence and the coding distribution diagram b, while the lower part is the corresponding simulation diagram c and d of the sequence. In this simulation comparison, the additive coded metasurface still plays a role in improving the reflection efficiency. By comparing the two sets of amplification, this addition principle can be adapted to the coded metassurfaces of different orders. Based on the generalized refraction and reflection law, the addition principle can always ensure that the new superunit sequence has the same diffraction angle as the original superunit by changing the size of the grating period and adding a new gradient phase superunit sequence in the process of using the addition principle.

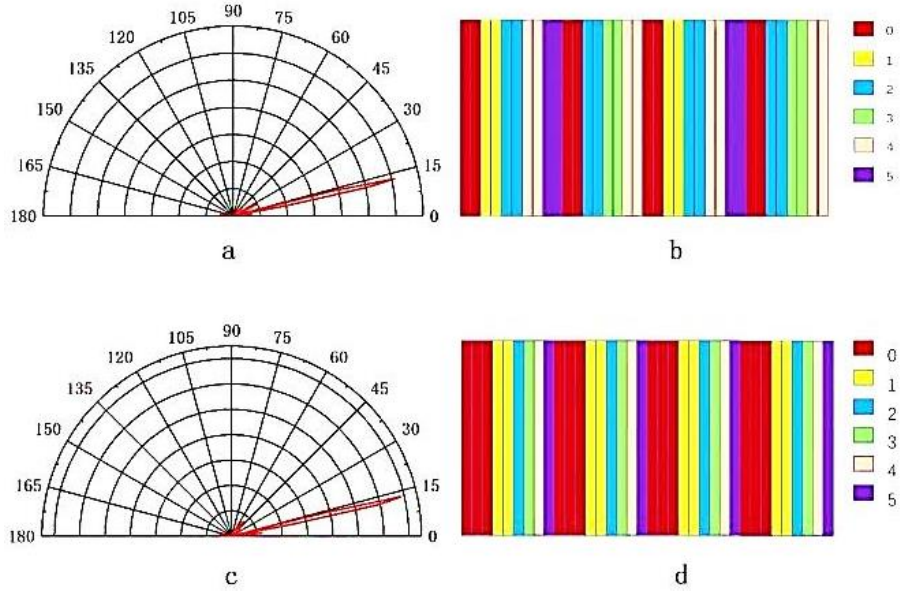


*Fig. 10. The basic sequence encodes the cell arrangement and the corresponding far-field scattering. (a) Far-field scattering of $S_0$, (b) Coding unit arrangement of $S_0$, (c) Far-field scattering of $S_m$, (d) Coding unit arrangement of $S_m$ (color online)*

Next, we construct a more complex coded sequence metasurface based on the addition principle. We build the coding sequences $S_0 = 012345\ldots\ldots$, $S_1 = 001233\ldots\ldots$, and $S_2 = 002244\ldots\ldots$. According to the encoding addition principle, $S_1$ can be obtained by adding $A_1 = 001122334455\ldots\ldots$, $A_2 = 000111222333444555\ldots\ldots$, and $A_3 = 000000111111222222333333444444555555$. $S_2$ can be obtained by adding $A_1 = 001122334455$ and $A_2 = 001122334455$. Although the superposition method is different, it still conforms to the addition principle and ensures the same diffraction direction. The encoding arrangements of the three coding sequences and the corresponding far-field scattering are shown in Fig. 11. It can be seen that the reflection efficiency of the new coded metasurface obtained by the two calculation methods is lower than that of the basic gradient phase coded metasurface, and the weakening degree is different.

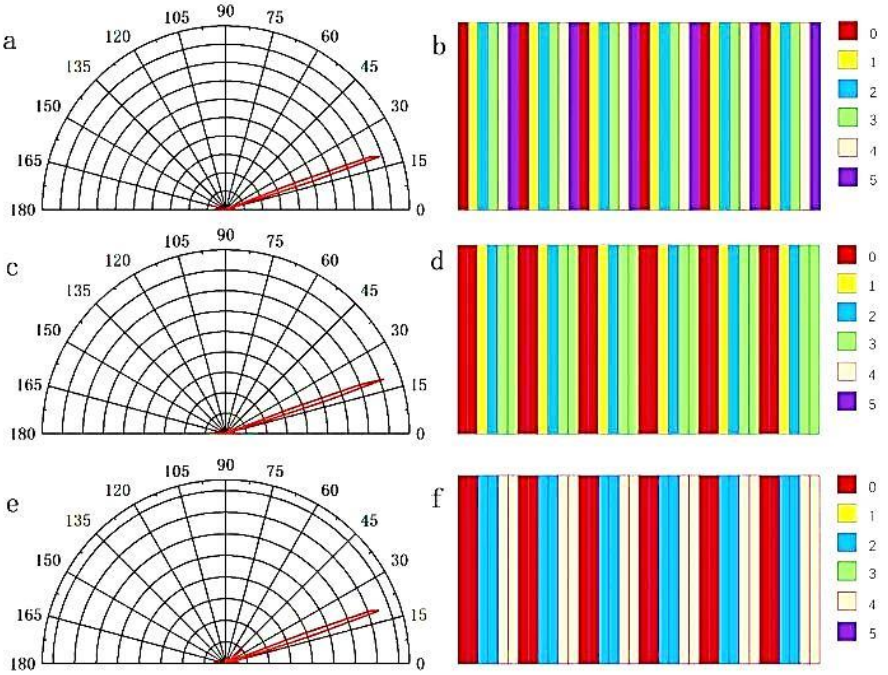


*Fig. 11. Coding arrangements and far-field scattering diagrams of coding sequences S0,S1 and S2 (color online)*

## 4. Conclusions

Based on the geometric phase principle, we design a kind of coding unit whose reflection phase can be continuously changed. This simple coding unit structure can be combined to build different coding sequences. Based on the coding addition principle, we construct several groups of different sequences of coded metasurfaces and control their scattering angles.

## References

[1] X. Jing, S. Jin, Y. Tian, P. Liang, Q. Dong, L. Wang, Optics & Laser Technology **48**, 160 (2013).
[2] X. Jing, Y. Xu, H. Gan, Y. He, Z. Hong, IEEE Access **7**, 144945 (2019).
[3] L. Jiang, B. Fang, Z. Yan, J. Fan, C. Qi, J. Liu, Y. He, C. Li, X. Jing, H. Gan, Z. Hong, Optics & Laser Technology **123**, 105949 (2020).
[4] Ziyu Liu, Limei Qi, Feng Lan, Chuwen Lan, Jun Yang, Xiang Tao, Chin. Opt. Lett. **20**, 013602 (2022).
[5] Shunshuo Cai, Wanhan Hu, Yiman Liu, Juan Ning, Sixuan Feng, Chao Jin, Lingling Huang, Xin Li, Chin. Opt. Lett. **20**, 053601 (2022).
[6] Chunyan Jin, Wei Wu, Lei Cao, Bofeng Gao, Jiaxin Chen, Wei Cai, Mengxin Ren, Jingjun Xu, Chin. Opt. Lett. **20**, 113602 (2022).
[7] Pengfei Wang, Fengyan He, Jianjun Liu, Fangzhou Shu, Bin Fang, Tingting Lang, Xufeng Jing, Zhi Hong, Photon. Res. **10**, 2743 (2022).
[8] Yang Zhu, Binbin Lu, Zhiyuan Fan, Fuyong Yue,

Xiaofei Zang, Alexei V. Balakin, Alexander P. Shkurinov, Yiming Zhu, Songlin Zhuang, Photon. Res. **10**, 1517 (2022).
[9] Bo Fang, Zhiyu Cai, Yandong Peng, Chenxia Li, Zhi Hong, Xufeng Jing, Journal of Electromagnetic Waves and Applications **33**(11), 1375 (2019).
[10] B. Fang, B. Li, Y. Peng, C. Li, Z. Hong, X. Jing, Microw. Opt. Technol. Lett. **61**, 2385 (2019).
[11] Weimin Wang, Xufeng Jing, Jingyin Zhao, Yinyan Li, Ying Tian, Optica Applicata **47**(2), 183 (2017).
[12] L. Jiang, B. Fang, Z. Yan, C. Li, J. Fu, H. Gan, Z. Hong, X. Jing, Microwave and Optical Technology Letters **62**(6), 2405 (2020).
[13] C. Gheorghiu, M. Cerchez, E. Aktan, R. Prasad, F. Yilmaz, N. Yilmaz, V. Leca, High Power Laser Science and Engineering **10**, 010000e3 (2022).
[14] G. Wang, J. Song, Y. Chen, S. Ren, P. Ma, W. Liu, P. Zhou, High Power Laser Science and Engineering, **10**, 04000e22 (2022).
[15] T. Liu, M. Zhu, W. Du, J. Shi, J. Sun, Y. Chai, J. Shao, High Power Laser Science and Engineering **10**, 05000e30 (2022).
[16] L. Jiang, Z. Yu, W. Zhao, Z. Yang, Y. Peng, Y. Zhou, X. Lin, S. Jin, Anal. Chem. **95**(2), 1721 (2023).
[17] Z. Yu, L. Jiang, R. Liu, W. Zhao, Z. Yang, J. Zhang, S. Jin, Chem. Eng. J. **426**, 131914 (2021).
[18] R. Liu, L. Jiang, Z. Yu, X. Jing, X. Liang, D. Wang, B. Yang, C. Lu, W. Zhou, S. Jin, Sensor Actuat. B-Chem. **333**, 129581 (2021).
[19] X. Jing, X. Gui, P. Zhou, Z. Hong, Journal of Lightwave Technology **36**(12), 2322 (2018).
[20] R. Xia, X. Jing, X. Gui, Y. Tian, Optical Materials Express **7**(3), 977 (2017).
[21] J. Zhao, X. Jing, W. Wang, Y. Tian, D. Zhu, G. Shi, Optics & Laser Technology **95**, 56 (2017).
[22] T.-J. Cui, M.-Q. Qi, X. Wan, J. Zhao, Q. Cheng, Light: Sci. Appl. **3**(10), e218 (2014).
[23] Xufeng Jing, Xiaoyan Tang,Ying Tian, Zhe Kong, Chenxia Li, Changyu Shen, Zhi Hong Journal of Lightwave Technology **40**(1), 136 (2022).
[24] Hong Bo Jing, Qian Ma, Guo Dong Bai, Tie Jun Cui, Advanced Optical Materials **7**(9), 1801742 (2019).
[25] Rui Yuan Wu, Chuan Bo Shi, Shuo Liu, Wei Wu, Tie Jun Cui, Advanced Optical Materials **6**(5), 1701236 (2018).
[26] Huifang Zhang, Xueqian Zhang, Quan Xu, Chunxiu Tian, Qiu Wang, Yuehong Xu, Yanfeng Li, Jianqiang Gu, Zhen Tian, Chunmei Ouyang, Xixiang Zhang, Cong Hu, Jiaguang Han, Weili Zhang, Advanced Optical Materials **6**, 1700773 (2018).
[27] Wenyun Du, Meiping Zhu, Jun Shi, Tianbao Liu, Jian Sun, Kui Yi, Jianda Shao, High Power Laser Science and Engineering **11**(5), 05000e61 (2023).
[28] Sunny Howard, Jannik Esslinger, Robin H. W. Wang, Peter Norreys, Andreas Döpp, High Power Laser Science and Engineering **11**(3), 03000e32 (2023).
[29] Karim Achouri, Ville Tiukuvaara, Olivier J. F. Martin, Advanced Photonics **5**(4), 046001 (2023).
[30] Zeyang Liu, Danyan Wang, Hao Gao, Moxin Li, Huixian Zhou, Cheng Zhang, Advanced Photonics **5**(3), 034001 (2023).
[31] Jiawei Yan, Gianluca Geloni, Advanced Photonics Nexus **2**(3), 036001 (2023).
[32] Nian Zhang, Baoxing Xiong, Xiang Zhang, Xiao Yuan, Advanced Photonics Nexus **2**(3), 036013 (2023).
[33] Quan Xu, Yuanhao Lang, Xiaohan Jiang, Xinyao Yuan, Yuehong Xu, Jianqiang Gu, Zhen Tian, Chunmei Ouyang, Xueqian Zhang, Jiaguang Han, Weili Zhang, Photonics Insights **2**(1), R02 (2023).
[34] Hyunjung Kang, Dohyeon Lee, Younghwan Yang, Dong Kyo Oh, Junhwa Seong, Jaekyung Kim, Nara Jeon, Dohyun Kang, Junsuk Rho, Photonics Insights **2**(2), R04 (2023).
[35] Jitao Li, Guocui Wang, Zhen Yue, Jingyu Liu, Jie Li, Chenglong Zheng, Yating Zhang, Yan Zhang, Jianquan Yao, Opto-Electron. Adv. **5**, 210062 (2022).
[36] Bo Bao, Yu Hua, Ridong Wang, Dachao Li, Adv. Quantum Technol. **6**(5), 2200146 (2023).
[37] Michael R. Geller, Adv. Quantum Technol. **6**(6), 2200156 (2023).
[38] H. Zhao, X. K. Wang, S. T. Liu, Y. Zhang, Opto-Electron. Adv. **6**, 220012 (2023).
[39] Hui Gao, Xuhao Fan, Yuxi Wang, Yuncheng Liu, Xinger Wang, Ke Xu, Leimin Deng, Cheng Zeng, Tingan Li, Jinsong Xia, Wei Xiong, Opto-Electron. Sci. **2**, 220026 (2023).
[40] Dianzhen Cui, Xuexi Yi, Li-Ping Yang, Adv. Quantum Technol. **6**(5), 2300037 (2023).
[41] Guoqing Wang, Francesca Madonini, Boning Li, Changhao Li, Jinggang Xiang, Federica Villa, Paola Cappellaro, Adv. Quantum Technol. **6**(9), 2300046 (2023).
[42] Yinhui Kan, Sergey I. Bozhevolnyi, Shailesh Kumar, Adv. Quantum Technol. **6**(12), 2300196 (2023).
[43] Yijia Huang, Tianxiao Xiao, Shuai Chen, Zhengwei Xie, Jie Zheng, Jianqi Zhu, Yarong Su, Weidong Chen, Ke Liu, Mingjun Tang, Peter Müller-Buschbaum, Ling Li, Opto-Electron. Adv. **6**, 220073 (2023).
[44] Jia Chen, Dapeng Wang, Guangyuan Si, Siew Lang Teo, Qian Wang, Jiao Lin, Opto-Electron. Adv. **6**, 220141 (2023).

*Corresponding author: cjlufangbo@163.com